Efficient XeF(C#A) laser oscillation using electron-beam excitation

Y. Nachshon, F. K. Tittel, and W. L. Wilson Jr.W. L. Nighan

Citation: Journal of Applied Physics **56**, 36 (1984); doi: 10.1063/1.333762
View online: http://dx.doi.org/10.1063/1.333762
View Table of Contents: http://aip.scitation.org/toc/jap/56/1
Published by the American Institute of Physics

Efficient XeF($C \rightarrow A$) laser oscillation using electron-beam excitation

Y. Nachshon, F. K. Tittel, and W. L. Wilson, Jr.
Electrical Engineering Department and Rice Quantum Institute, Rice University, Houston, Texas 77251

W. L. Nighan
United Technologies Research Center, East Hartford, Connecticut 06108

(Received 15 November 1983; accepted for publication 6 February 1984)

Significantly improved XeF($C \rightarrow A$) laser energy density and efficiency have been obtained using electron-beam excited Ar-Xe gas mixtures at pressures up to 10 atm which contain both NF_3 and F_2. Maximum blue-green laser pulse energy density in excess of 1.0 J/liter was obtained, corresponding to an intrinsic electrical-optical energy conversion efficiency estimated to be in the 0.5%–1.0% range. Comprehensive, time-resolved absolute measurements of XeF($C \rightarrow A$) fluorescence, laser energy, and gain were carried out for a wide variety of experimental conditions. Analysis of these data has resulted in identification of the dominant transient absorbing species in the laser medium. For the laser mixtures investigated in this work, the primary blue/green absorption processes have been identified as photoionization of the 4*p*, 3*d*, and higher lying states of Ar, and of the Xe 6*p* and 5*d* states, and photodissociation of $Ar_2(^3\Sigma_u^+)$ and Ar_3^+.

I. INTRODUCTION

Of the rare-gas halide molecules, XeF is unique in that the two lowest Coulombic states B ($\Omega = 1/2$) and C ($\Omega = 3/2$) are separated in energy by nearly 0.1 eV, XeF(C) being lower in energy of the two,[1] as illustrated in Fig. 1. Therefore, in thermal equilibrium at 300 °K more than 95% of the combined population of the B and C states resides in the latter. For this reason the broadband XeF($C \rightarrow A$) transition, centered near 490 nm, has potential for development of efficient tunable lasers in the blue/green region of the spectrum. Laser oscillation has been reported by a number of investigators using electron-beam excitation [2,3] or discharge excitation[4,5] of high-pressure gas mixtures containing Xe and a fluorine donor such as F_2 or NF_3. Additionally, laser oscillation based on photolytic pumping of a gas containing XeF_2 has been demonstrated.[6–8] For the conditions of these studies the laser output has been found to be continuously tunable in the 450–520 nm wavelength region.[7,9,10]

Although the XeF(C) excimer can be formed efficiently under conditions typical of these experiments, the large (~70 nm) $C \rightarrow A$ bandwidth and relatively long C-state lifetime (~100 nsec) result in a cross section for stimulated emission[7] that, at $\sim 10^{-17}$ cm^2, is more than an order of magnitude smaller than that of the highly efficient 351-nm $B \rightarrow X$ laser transition.[11] Thus, development of adequate gain on the $C \rightarrow A$ transition requires very intense pumping, a circumstance that results in high concentrations of electrons and of excited and ionized species when electrical excitation is used. The electrons tend to mix and quench the closely spaced B and C states, an effect strongly favoring the UV $B \rightarrow X$ transition at the expense of the blue/green $C \rightarrow A$ transition. More importantly, certain excited and ionized species typical of the laser medium absorb in the blue/green region of the spectrum. Until recently these and related factors have limited the efficiency of the electrically excited XeF($C \rightarrow A$) laser to unacceptably low levels.[2–5] Photolytic pumping of XeF_2-containing mixtures has been successful at circumventing certain of these effects, but at the expense of an increase in system complexity.[8]

Recently we reported results[1,2] demonstrating that by judicious tailoring of kinetic processes in electron-beam excited laser mixtures containing *both* NF_3 and F_2, the concentrations of electrons and of absorbing species could be significantly reduced. The resulting increase in laser pulse energy density and intrinsic efficiency to ~0.1 J/liter and ~0.1%, respectively, represented an improvement of nearly two orders of magnitude over previously reported results. Herein we report further improvements in laser energy density and efficiency, based primarily on increased *e*-beam energy deposition in the laser mixture and optimization of the output coupling. Additionally, analysis of comprehensive time-resolved measurements of gain and absorption for a wide variety of mixture conditions has provided insight as to the identity of the primary absorbing species and, in certain cases, has permitted estimation of their absorption cross sections.

The details of the experimental arrangement and related diagnostic apparatus used in this investigation are summarized in Sec. II. In Sec. III experimental results are presented; therein are described the specific conditions resulting in an increase in XeF($C \rightarrow A$) laser pulse energy density to the

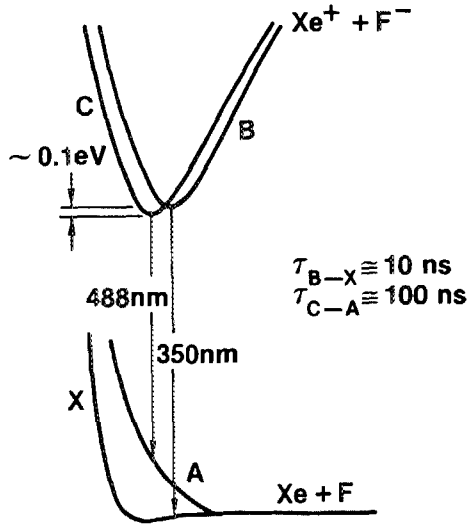

FIG. 1. Schematic XeF energy level diagram.

 0021-8979/84/130036-13$02.40

1.0–2.0 J/liter level, corresponding to an intrinsic efficiency estimated to be in the 0.5%–1.0% range. Our analysis and interpretation of those results is presented in Sec. IV–VI, wherein particular emphasis is placed on identification of the ionized and excited species dominating transient absorption in the XeF($C \rightarrow A$) laser mixture. Additionally, remaining factors that presently limit laser performance are discussed, along with possibilities for further improvement.

II. EXPERIMENT

A. Electron-beam and reaction cell

The overall experimental arrangement used in this investigation is illustrated in Fig. 2. A Physics International Pulserad 110 electron beam generator was used to transversely excite the high pressure laser mixtures through a 50-μm titanium foil (Fig. 3). The electron beam energy was 1 MeV and the pump pulse duration was 10 nsec (FWHM), producing a current density at the center of the optical axis of 200–400 A cm^{-2} as measured with a Faraday cup probe. A stable, intracell optical resonator was used consisting of a totally reflecting ($R > 99.6\%$) mirror having a radius of curvature of 0.5 m, separated by 12.5 cm from a flat output mirror. The output mirrors had a reflectivity of either 95% or 98% between 460 and 510 nm, thereby providing an optimum wavelength match with the XeF($C \rightarrow A$) gain profile. The active region was the cylindrical 28 cm^3 volume defined by the clear aperture (1.9 cm diam) and the pumped length (10 cm), as confirmed by photographs of the near field laser output. Use of a tightly focused resonator permits a higher level of initial flux arising from spontaneous emission, a factor contributing to rapid buildup of intracavity laser flux.

The stainless-steel reaction cell was well passivated by prolonged exposure to F_2 prior to any experiments. High-purity gas mixtures of research grade Ar, Xe, Kr, NF_3, and F_2 were used, with the F_2 in a 10–90 F_2-He mixture. Good mixing of the different gas components was achieved by turbulent flow of the high pressure gas components into the reaction cell. The concentration of F_2 in the cell was verified by absorption of a HeCd laser probe[13]; the partial pressure of each gas is estimated to be accurate to within 2%. A fresh gas mixture was used for each shot. Repetitive pumping of the mixture resulted in a decrease in laser energy of about 20% per shot due to contamination and surface reaction processes of the foil window.

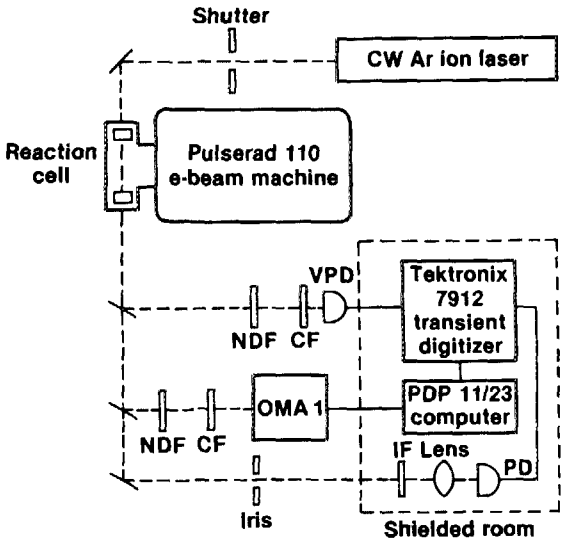

FIG. 2. Schematic illustration of experimental arrangement. NDF = neutral density filter, CF = color-glass filter, VPD = vacuum photodiode, PD = pin diode.

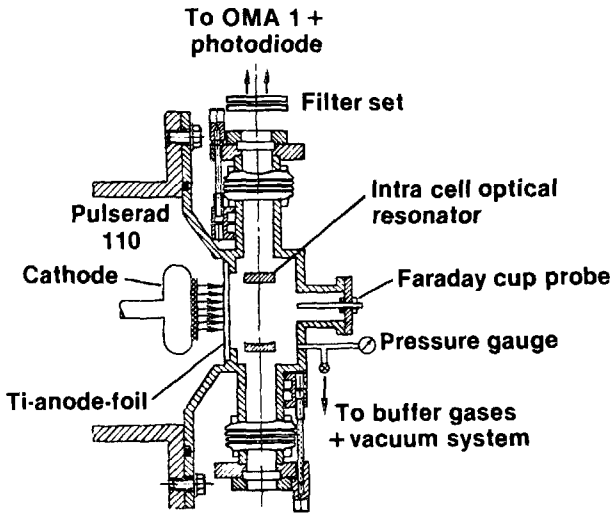

FIG. 3. Illustration of the transverse, e-beam excited high pressure reaction cell with an intracell optical cavity.

B. Diagnostics

The temporal evolution of the fluorescence and the laser output were monitored by a fast vacuum photodiode detector (ITT:F4000 S5). Neutral density, interference, and color glass filters were used to define the spectral region of interest. Signals with a time resolution of better than 2 nsec were recorded by a Tektronix 7904 Transient Digitizer. The temporally integrated, spectrally resolved fluorescence was recorded by an optical multichannel analyzer (OMA I), using a Jarrell-Ash 0.25 m spectrometer; the spectral resolution was ~2 nm. Data from the Transient Digitizer and the OMA I were processed using a PDP 11/23 minicomputer.

Absolute power measurements were made using calibrated vacuum photodiode detectors (with an effective aperture of 38 mm), and appropriate interference and color glass filters. The power was calculated using the temporally integrated OMA measurements and the calibration verified by means of a Scientech volume absorbing disc calorimeter model 38-0101 as well as with Polaroid film No. 42. The film was exposed to the laser output using neutral density and color glass filters to achieve a density of 0.5. These two methods of power determination were found to agree to within the estimated experimental error.

The laser beam divergence was also measured using two different methods. The first method used Polaroid film exposed to the laser light at different distances using neutral density and color glass filters, keeping the film density 0.5, and measuring the beam diameters. The second method measures the laser power at different distances along the optic axis for different size apertures. Both methods indicated a laser beam divergence of ~40 mrad.

A measurement of the temporal evolution of the XeF(C) population for different gas mixture conditions was carried out by monitoring the XeF($C \rightarrow A$) fluorescence at a distance 125 cm from the center of the laser cell along the optical axis using collimating optics with an effective aperture of 6.35 mm diam. The absolute value of the XeF(C) state population was then obtained using the integrated fluorescence spectrum from the OMA and the spectrally calibrated vacuum photodiode detector.

C. Gain/absorption measurement

The experimental arrangement for measuring the optical gain (absorption) is also shown in Fig. 2. A cw Ar-ion laser and an R 6G dye laser were used to measure gain at eight different wavelengths: 514.5, 501.7, 496.5, 488.0, 476.5, 472.7, 457.9, and 590 nm. Either one or three passes of the probe beam through the cell was used, depending on the magnitude of the gain/absorption, in order to maximize the signal-to-noise ratio. The laser probe signal was focused on a Lasermetrics 3117 PIN detector (HP5082-4200) via a narrow-band interference filter, color-glass filter, and an iris located 10 m from the laser cell. The detector was located inside a Faraday cage to minimize electrical noise pickup and stray fluorescence. A mechanical shutter was used to produce a 4-msec laser probe pulse to avoid saturation of the detector. The electron-beam pulse was synchronized to appear in the middle of the laser probe pulse. In the cw mode, the detector diode is linear with input power for output currents up to 4 mA. However, the time response of the detector for currents above 2 mA started to deteriorate. Therefore, the detector current was always maintained below 1 mA, where the time response is estimated to be better than 2 nsec.

III. EXPERIMENTAL RESULTS

Normalized temporal characteristics of the e-beam excitation pulse, XeF($C \rightarrow A$) fluorescence and laser output for representative conditions are presented in Fig. 4. Formation of the XeF(C) state occurs during and after the excitation pulse, with the fluorescence peak occurring about 10 nsec after the peak in the e-beam current. Since there is strong absorption during the early phase of XeF(C) formation (a topic to be discussed in detail in subsequent sections), laser oscillation does not begin until after the peak fluorescence. The peak in the laser output occurs between 20 and 35 nsec after the fluorescence peak depending on the magnitude of the peak gain, the shorter time corresponding to higher gain, and therefore higher laser output. Laser oscillation continues for 20–30 nsec after termination of the XeF($C \rightarrow A$) fluorescence, a reflection of the cavity resonator decay time.

A. Laser pulse energy

The improvement in magnitude and duration of the net gain resulting from a two component halogen donor mixture (NF_3/F_2) has been shown to result in a significant increase in laser pulse energy.[12] Figure 5 presents the laser pulse energy density (based on a 28 cm^3 active volume) as a function of *either* F_2 pressure or NF_3 pressure for 10 atm of Ar containing 16 Torr Xe; a 2% output coupler was used. The maximum output of 0.5 J/liter for these specific conditions is observed to occur for a mixture containing 8 Torr of NF_3 and 8 Torr of F_2, and is particularly sensitive to the concentration of the latter, a reflection of the fact that F_2 has substantially larger excited state (i.e., absorber) quenching coefficients than does NF_3.[14,15] For conditions similar to those of Fig. 5 maximum laser pulse energy density values of 1.5 J/liter were achieved using a 5% output coupler.

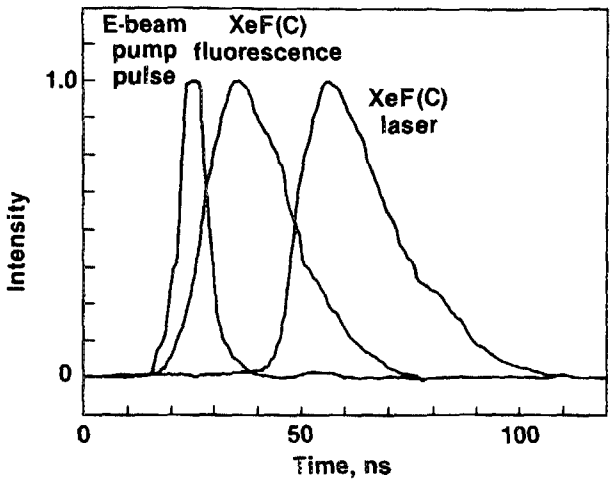

FIG. 4. Normalized temporal characteristics of the e-beam excitation pulse, XeF($C \rightarrow A$) fluorescence, and laser pulse for a mixture comprised of 10 atm Ar, 16 Torr Xe, 8 Torr NF_3, and 8 Torr F_2. The e-beam current density on the optical axis was approximately 400 A cm^{-2}, and the transmission of the output mirror was 2%.

Optimum mixtures were always found to contain about 8 Torr NF_3, 8 Torr F_2, and 16 Torr Xe, regardless of the cavity optics, e-beam current density, or Ar pressure. Thus, the concentrations of NF_3, F_2, and Xe are essentially optimized for the present conditions. However, the e-beam current density (~400 A/cm^2 max) and Ar pressure (10 atm max), corresponding to the highest measured laser output (~1.5 J/liter), represent experimental limitations and are not optimum values. For values of e-beam current density between 200 and 400 A cm^{-2} and Ar pressures between 6 and 10 atm, laser pulse energy density increased somewhat faster then linearly with each of these parameters. However, for values below about 200 A cm^{-2} and 6 atm, laser pulse

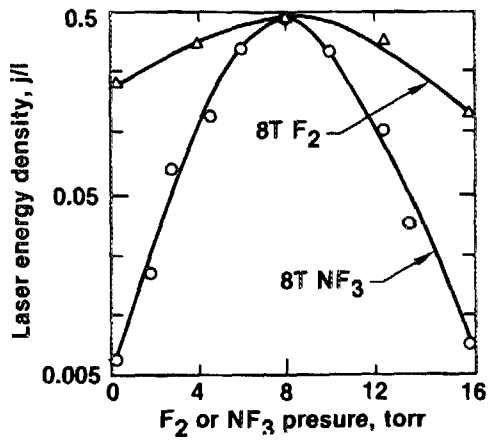

FIG. 5. Laser pulse energy density as a function of *either* NF_3 pressure or F_2 pressure for conditions otherwise the same as Fig. 4.

energy was found to decrease very rapidly due to the lower gain under these conditions.

1. Buffer gas variation

Use of Ne as the buffer gas in place of Ar resulted in laser pulse energy much lower than that of Fig. 5, almost certainly a reflection of the fact that Ne is about an order of magnitude less effective than Ar at mixing the B and C states of XeF,[16] and is also less effective at relaxing the XeF(B,C) vibrational manifolds. The use of Kr in place of Ar was reported[3] to result in much better laser performance for values of e-beam current density and total pressure much lower and excitation pulses much longer than those of the present investigation. However, we have found that use of Kr as the buffer at half the Ar pressure, so as to provide about the same e-beam energy deposition, resulted in significantly lower laser output energy. Experimentation using Kr as an *additive* at concentrations in the 0–760 Torr range was also found to result in lower laser output, except for Kr pressures in the 40–70 Torr range for which the laser output was about the same as without Kr present. However, measured gain profiles in laser mixtures containing Kr feature certain distinctive characteristics that may ultimately permit higher laser pulse energy, a topic to be discussed in subsequent sections.

2. Laser spectra

Although the laser output was found to be quite sensitive to mixture variations, the XeF($C\rightarrow A$) fluorescence was not, a circumstance indicating that changes in the absorption characteristics of the medium are largely responsible for changes in laser output. Examination of laser spectra supports this conclusion. Figure 6 shows measured laser spectra for an Ar-Xe mixture at 6 atm containing 8 Torr NF_3, and 8 Torr each of F_2 and NF_3, excited at an e-beam current density level of about 200 A cm^{-2}, conditions for which the laser pulse energy density was about 0.1 J/liter for the two-halogen mixture.[12] The discrete absorption lines that appear in the NF_3 spectrum [Fig. 6(a)], due principally to transitions between Xe excited states,[17] vanish [Fig. 6(b)] with F_2 added to the mixture for laser output energy up to about 0.1 J/liter. For higher laser pulse energy (e.g., Fig. 5) the structure in the laser spectrum is again apparent even with F_2 present in the mixture, although to a much lesser degree than with NF_3 alone. For this case the laser pulse peaks at an earlier time at which the absorber concentrations are higher than those typical of Fig. 6(b).

It should be pointed out that the effect of broadband absorption on laser output energy is far more significant than that of the discrete absorption that is readily apparent in the laser spectrum [Fig. 6(a)]. However, many of the same species contributing to broadband absorption also exhibit discrete absorption. For this reason the appearance of structure and/or changes therein in XeF($C\rightarrow A$) laser spectra [Figs. 6(a) and 6(b)] are also symptomatic of the occurence of the more severe broadband absorption.

B. Gain and absorption

Figure 7 presents the temporal evolution of net gain at 488 nm (measured using the cw Ar-ion laser probe) for a laser

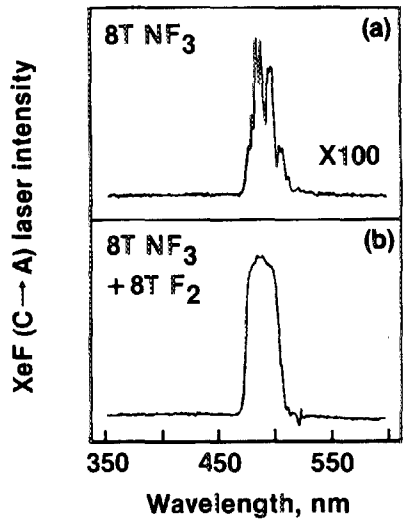

FIG. 6. XeF($C\rightarrow A$) laser spectra for a mixture of 6 atm Ar and 16 Torr Xe containing 8 Torr NF_3 (a), or 8 Torr NF_3 and 8 Torr F_2 (b). The e-beam current density on the optical axis was approximately 200 A cm^{-2} and the transmission of the output coupler was 5%. For these conditions, the laser pulse energy density was about 0.1 J/liter.

mixture for which the Ar pressure was 6 atm. Under these conditions laser output energy density was about 0.25 J/liter. This figure shows that severe transient absorption occurs during the excitation pulse, a circumstance found to be typical of all Ar-Xe-NF_3-F_2 laser mixtures. The net gain does not become positive until slightly before the peak in the fluorescence. For an Ar pressure of 10 atm, corresponding to $\sim$1.0–2.0 J/liter laser output, the peak absorption rises to nearly 4% cm^{-1} and the peak gain increases to almost 3% cm^{-1} (Fig. 8). The peak values of the XeF(C) population deduced from the gain measurements (and predicted analytically) typically were about 25% larger than those determined from the calibrated fluorescence measurements, a difference within the combined uncertainty limits of both experimental techniques.

For the conditions of Fig. 7 (e.g., peak gain $\gtrsim$ 2% cm^{-1}) the maximum intracavity laser flux corresponds to values equal to or greater than the saturation flux, $I_{sat} \sim 6$ MW cm^{-2}. Thus, while the laser output energy continues to

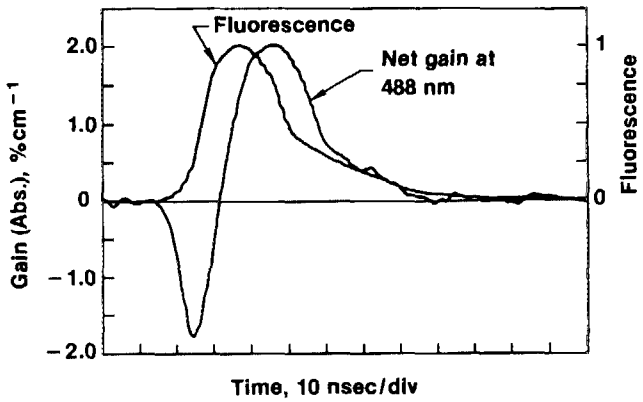

FIG. 7. Temporal evolution of the net gain measured at 488 nm and of the fluorescence for a mixture comprised of 6 atm Ar, 16 Torr Xe, 8 Torr NF_3, and 8 Torr F_2; the e-beam current density on the optical axis was approximately 300 A cm^{-2}.

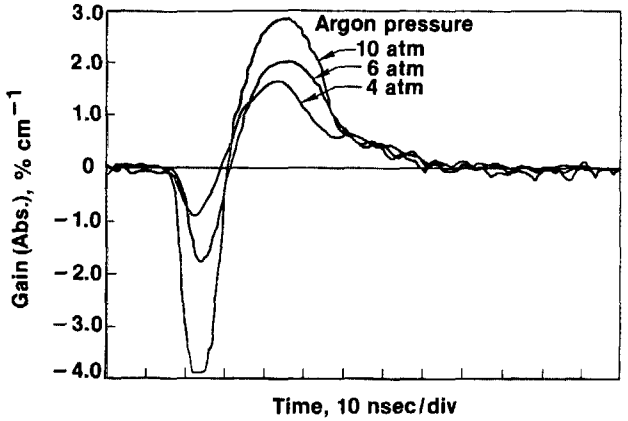

FIG. 8. Temporal evolution of the net gain measured at 488 nm for various Ar pressures, and conditions otherwise the same as those of Fig. 7.

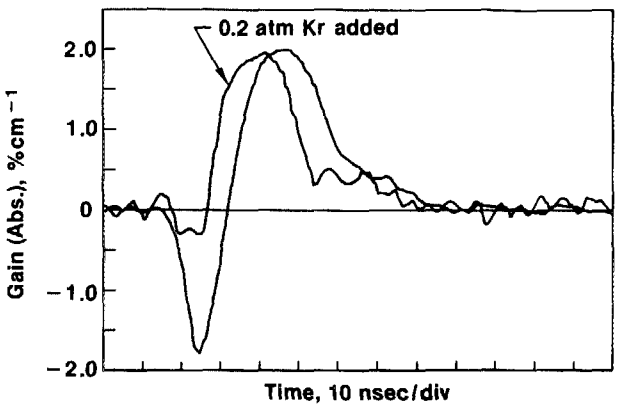

FIG. 10. Temporal evolution of the net gain at 488 nm for the conditions of Fig. 7, and for those conditions with 0.2 atm Kr added to the mixture.

increase significantly for peak gain levels higher than those of Fig. 7, for lower gain values (e.g., $\lesssim 1.5\%$ cm^{-1}) the laser output energy decreases precipitously. Figure 9 compares the gain for the two-halogen mixture of Fig. 7 with that of a mixture containing only NF_3; both excited under similar conditions. In the latter case the broadband absorption is more severe resulting in a gain peak of about 1.5% cm^{-1}. However, because these gain values are relatively low, considering the 30 nsec during which gain persists, the difference in laser pulse energy between the $F_2 + NF_3$ and NF_3 mixtures is approximately two orders of magnitude (Fig. 5).

Although Kr did not improve laser performance for the conditions of this experiment, the addition of Kr to the laser mixture was found to have a striking effect on the temporal evolution of the gain-absorption profile under certain circumstances. Presented in Fig. 10 is the net gain at 488 nm for the mixture of Fig. 7, to which was added 0.2 atm Kr. While the peak value of gain is essentially the same for both cases, the strong initial absorption during the excitation pulse almost vanishes entirely. This was found to be the case for all Kr concentrations in the 0.2–1.0 atm pressure range. For Kr pressures above 1.0 atm the initial absorption was found to return to significant levels, and the peak gain decreased. With the Ar replaced entirely by 3 atm Kr, the initial absorption increased to nearly 1.0% cm^{-1} and the peak value of gain decreased to approximately 1.5% cm^{-1}. Thus, for the conditions of this experiment, the use of Kr as an *additive* rather than as the buffer has an interesting and potentially significant effect on blue/green absorption during the excitation pulse, a topic to be explored in subsequent sections.

1. Wavelength dependence

As mentioned earlier, broadband absorption is of central importance to laser performance. For this reason gain/absorption measurements of the type discussed above were carried out for seven wavelength values available from the cw Ar-ion laser, and for the 590-nm R 6G dye laser wavelength. Presented in Fig. 11 is the wavelength dependence of the peak gain and peak absorption for the mixture and excitation conditions of Fig. 7, measured using the Ar-ion laser. The curve in this figure is the XeF($C \rightarrow A$) stimulated emission cross section reported in Ref. 7, normalized to the measured peak gain value at 480 nm. With the exception of the point at 514.5 nm,[18] the peak absorption is found to be essentially independent of wavelength. Thus, the decrease in the peak value of net gain on either side of 480 nm is primarily a reflection of the wavelength dependence of the $C \rightarrow A$ cross section for stimulated emission.

IV. XeF($C \rightarrow A$) LASER KINETICS

In recent years kinetic processes controlling the XeF(B,C) population in laser media have been the subject of

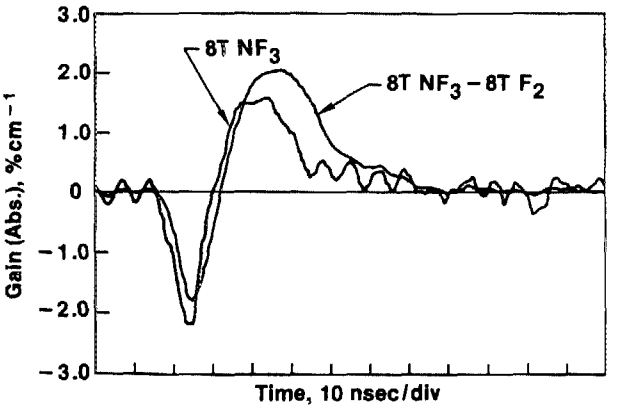

FIG. 9. Temporal evolution of the net gain at 488 nm for the conditions of Fig. 7, and for those conditions with no F_2 in the mixture.

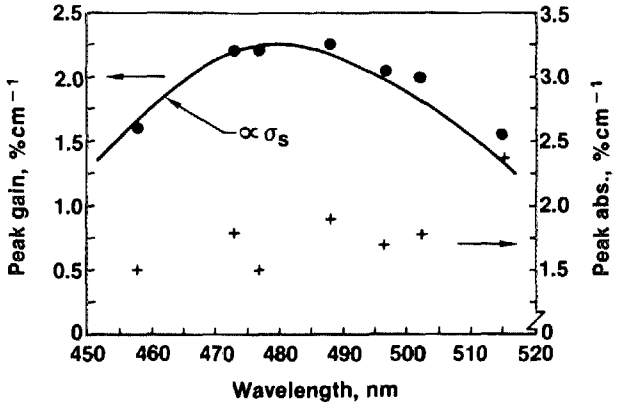

FIG. 11. Wavelength dependence of the peak gain and peak absorption for the conditions of Fig. 7. The curve refers to the wavelength dependence of the XeF($C \rightarrow A$) cross section for stimulated emission reported in Ref. 7.

considerable attention. Consequently, relatively complete rate coefficient data are available for XeF(B,C) formation processes such as ion-ion recombination[19,20] and halogen reactive quenching of rare-gas excited states[14,15] and for mixing and quenching of the B and C states.[16,21] Additionally, the body of related data pertaining to ion charge exchange and rearrangement,[22–24] kinetic processes in rare gases and their mixtures,[25,26] and to electron-halogen dissociative attachment[27] has been expanded significantly in reaction to the importance of rare-gas-halide lasers. In the present investigation these data have been used in a self-consistent model of XeF(B,C) processes for the experimental conditions described in Sec. III. Analytical and numerical procedures of the type utilized have become well developed in recent years.[28,29] Thus, the discussion to follow will concentrate on modeling results with little emphasis on methods and procedures.

A. Mixture composition

Selection of an optimum buffer gas for the XeF($C \rightarrow A$) laser is dictated by several requirements: (1) mixing of the B and C states must occur in a time much less than the radiative lifetime of the former; (2) vibrational relaxation of the B and C states must be very fast: (3) collisional quenching of XeF by the buffer must be minimal; (4) transient absorption at the laser wavelength by buffer-related ionized and excited species must be held to an acceptable level; and (5) when e-beam excitation is used the buffer gas must have a relatively high stopping power. While there are several species possessing one or more of these characteristics, so far Ar has been found to exhibit the best overall combination of properties for the conditions of this experiment.

The molecular source of fluorine atoms should also possess properties (3) and (4) above, and since net gain and laser oscillation occur during the afterglow period and are strongly influenced by absorption in the relaxing medium, the halogen must play the very important role of reducing the concentrations of electrons and absorbing species as rapidly as possible. As mentioned previously and discussed in detail in Ref. 12, we have shown that F_2 and NF_3 together exhibit attachment and absorber quenching characteristics superior to either species alone, thereby permitting higher levels of net gain and very much higher laser pulse energies. Most recently, evidence has been obtained indicating that addition of Kr as a fifth component of the mixture may beneficially alter medium absorption characteristics. These reasons and supportive experimental evidence have resulted in selection of the particular mixture constituents and their fractional concentrations described previously in connection with the discussion of Figs. 5–11.

B. XeF(C) formation and loss

Figure 12 illustrates the major energy pathways to and away from the coupled XeF(B,C) vibrational manifolds, based on modeling of kinetic processes. Because of the very large fractional concentration of Ar, ionization and excitation of the Ar by primary and secondary e-beam electrons is dominant, followed by charge and excitation transfer to Xe, and by ion recombination and excited state quenching by F^-

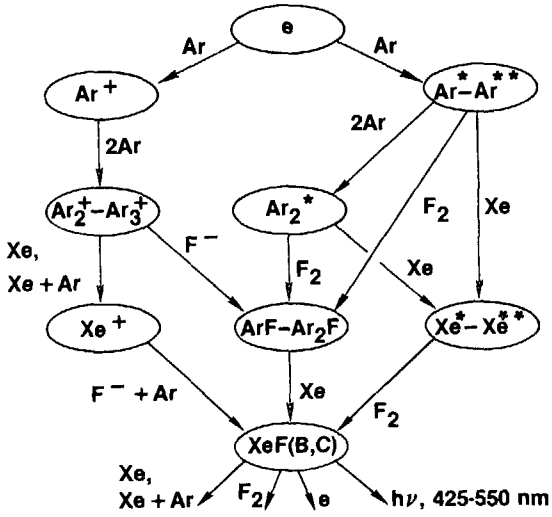

FIG. 12. Sequence diagram illustrating the XeF(B,C) formation and loss processes for the conditions of the present investigation.

and by F_2 (and NF_3), respectively. Those processes resulting in the formation of Xe ions and/or Xe excited states result in very efficient formation of XeF(B,C).[14,19] However, the indicated paths leading to ArF and Ar_2F introduce inefficiency even though a fraction of that energy is also likely to result in XeF formation by way of displacement reactions. Nevertheless, modeling indicates that for the conditions of this experiment XeF(C) is produced with an efficiency of 5%–7% for a relatively wide range of experimental conditions.

The computed, time integrated fractional contributions to XeF(C) formation and loss are presented in Fig. 13, for conditions typical of Fig. 7. Because Ar mixes the XeF states on a sub-nsec time scale,[16] it doesn't matter whether the B, C or D state of XeF is produced by the reactions indicated in Fig. 13(a). Of those reactions, the relative importance to XeF formation of the Ar_2F-Xe displacement reaction is least certain. A substantial fraction of the energy is channeled to ArF (Fig. 12) which is instantly converted to Ar_2F because of the high Ar pressure.[30] While there is evidence of displacement

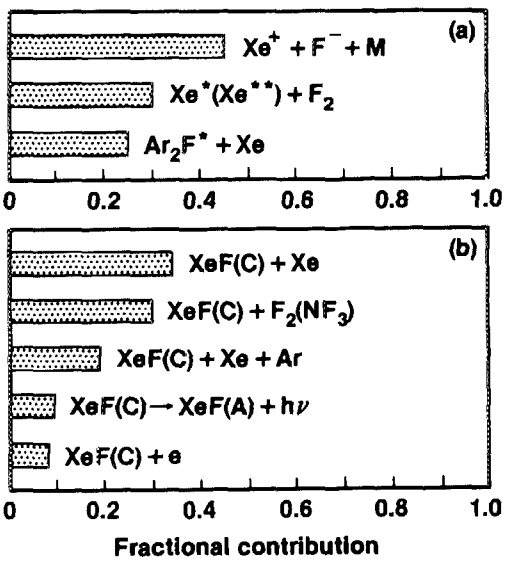

FIG. 13. Time integrated fractional contributions to XeF(C) formation (a), and loss (b), computed for the conditions of Fig. 7.

reactions involving diatomic rare-gas-halide moledules, there is very little information on the corresponding triatomic molecule reactions.[29] For the purposes of the present calculations the rate coefficient for the $Ar_2F \rightarrow XeF$ displacement reaction was estimated to be 2×10^{-10} sec^{-1} cm^3.

The contributions to XeF(C) quenching are presented in Fig. 13(b), which shows that nearly 50% of the C state loss is due to two- and three-body quenching[21] by Xe, a factor that limits the Xe fractional concentration to a relatively low level. Also, in spite of the very large rate of dissociative attachment in the NF_3-F_2 mixture, the intense e-beam pumping results in an electron density level such that electron quenching of the XeF(B,C) states is still significant.[31]

V. ABSORPTION IN THE VISIBLE REGION

Although the kinetic efficiency for production of the upper laser level may be relatively high for excimer systems, ~5%-7% in the present case, the overall laser efficiency can be severely limited by photoabsorption.[32–35] In recognition of this fact and the importance of UV rare-gas and rare-gas-halide lasers, in recent years there has been significant activity directed toward identification of species in laser media that absorb in the UV, and toward determination of their cross sections. For this reason transient absorption processes in electrically excited UV laser media are now relatively well understood.[32] Unfortunately, far less is known about the causes of the absorption observed in the visible region of the spectrum.[36] Since control of absorption in the blue/green region is absolutely critical to efficient operation of the XeF($C \rightarrow A$) laser, we have endeavored to identify the specific causes of the broadband absorption observed in the present experiment. Progress toward this objective has been aided significantly by analysis of the absorption characteristics of specific rare gas mixtures in addition to the XeF laser mixtures of primary interest.

A. Argon

Presented in Fig. 14 is the time dependence of the absorption measured at 488 nm in argon for conditions otherwise typical of the laser experiments discussed in Sec. III. The magnitude of the peak absorption, ~9% cm^{-1}, was found to be about the same at 457.9 nm and approximately 30% higher[18] at 514.5 nm, indicating that the absorption is essentially broadband in nature. Analysis of the decay of the absorption in Ar shows it to be composed of two components having characteristic times of approximately 15 and 50 nsec, respectively, a trend also observed by others[36] for generally similar conditions. Model calculations for the conditions of Fig. 14 provide valuable insight as to the excited and ionized species responsible for the Ar absorption, and permit first-order estimates of absorption cross sections for which data are unavailable.

Computed species concentrations corresponding to the conditions of Fig. 14 are presented in Fig. 15. Here Ar* refers to the population of the Ar(4s) levels as indicated, while Ar** refers to a single, effective higher-lying state representative of the grouped 4p, 3d and higher levels. The computed concentration of the weakly bound (D_e ~0.22 eV) Ar_3^+ trimer ion is based on the forward and reverse rate coefficients reported by Turner and Conway,[37] and on the assumption that the rate coefficient for electron-Ar_3^+ recombination is five times larger[38] than that of Ar_2^+. Examination of Fig. 15 shows that, with the exception of $Ar_2^*(^3\Sigma_u^+)$, all other species essentially follow the temporal behavior of the e-beam excitation pulse, and decay with a time constant of about 10–20 nsec. In contrast, the long lived (~3 μsec) Ar_2^* ($^3\Sigma_u^+$) state decays by way of electron mixing with the $Ar_2^*(^1\Sigma_u^+)$ state, the latter having a lifetime of only 4 nsec.[39] Although the $^1\Sigma_u^+$ concentration is always much smaller than that of $^3\Sigma_u^+$, spontaneous emission of the former provides the path through which the coupled (by electrons) $^1\Sigma_u^+ - {}^3\Sigma_u^+$ states decay. For these reasons the computed 40–50 nsec decay time constant of Ar_2^* ($^3\Sigma_u^+$) reflects the electron density decay rather than the $^3\Sigma_u^+$ lifetime.

For the species of Fig. 15 the dominant *broadband* photoabsorption processes in the blue/green region are expected to be

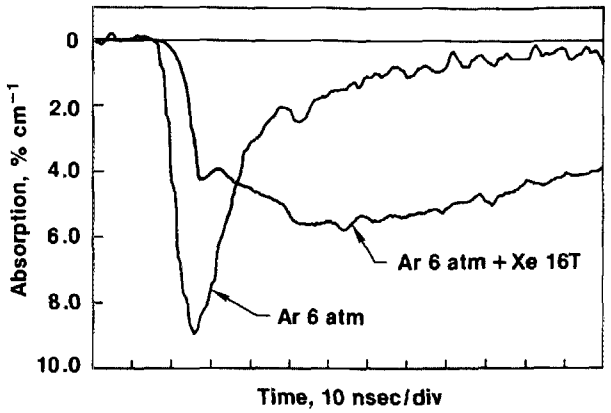

FIG. 14. Temporal evolution of the absorption measured at 488 nm in 6 atm Ar and in 6 atm Ar containing 16 Torr Xe. The e-beam current density was approximately 300 A cm^{-2}.

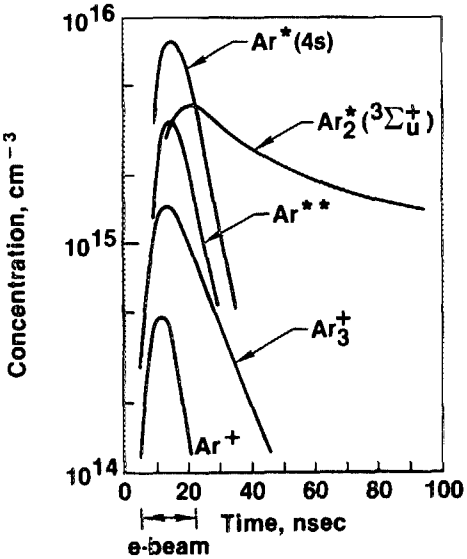

FIG. 15. Computed temporal evolution of the species concentrations in Ar for the conditions of Fig. 14. The peak value of the Ar_2^+ concentration (not shown for the sake of clarity) is approximately three times larger than that of Ar_3^+.

$$h\nu + Ar^{**} \rightarrow Ar^{+} + e, \quad (1)$$

$$h\nu + Ar_3^{+} \rightarrow Ar^{+} + 2Ar, \quad (2)$$

$$h\nu + Ar_2^{*} \rightarrow Ar^{**} + Ar. \quad (3)$$

Duzy and Hyman[40] have computed cross sections for the photoionization process, [Eq. (1)]. Although photons in the blue/green region have insufficient energy to ionize Ar*(4s) atoms, they report photoionization cross sections of $\sim 1.2\times10^{-17}$ cm^2 for Ar**(4p) for $\lambda \lesssim 460$ nm, and $\sim 1.5\times10^{-17}$ cm^2 for Ar**(3d) for $430 \lesssim \lambda \lesssim 530$ nm. Presumably the cross sections for photoionization of higher excited states are somewhat larger. Cross sections for dimer ion (Ar_2^+) photodissociation peak in the UV region.[41] Although absorption in the blue/green by Ar_2^+ in high vibrational levels is possible, dimer ion absorption is not likely to be significant at the pressure levels of the present experiment. However, recent calculations by Michels, Hobbs, and Wright[42] and by Wadt[43] show that photodissociation of rare gas *trimer* ions is likely to be very strong and broadband throughout most of the visible region. Michels and coworkers report a cross section for Ar_3^+ that is approximately 10^{-17} cm^2 in the blue/green region, while Wadt's calculations suggest that the cross section may be substantially larger than that.[44] Although there are no reported cross sections for blue/green photoabsorption by Ar_2^*, recent calculations[45] by Yates and co-workers show that several molecular states correlating to Ar-Ar(4p) are highly repulsive in the region of the equilibrium internuclear separation of Ar_2^* ($^3\Sigma_u^+$), and have vertical transition energies in the 2-4 eV range. This suggests the possibility of significant broadband absorption by Ar_2^* in the visible region.

This information, considered in light of both the computed temporal evolution of excited and ionized species in Ar (Fig. 15), and of the measured absorption (Fig. 14), indicates that the strong initial absorption during the excitation pulse is caused by the combined effects of the 4p, 3d, and higher excited states of Ar, by Ar_3^+, and by $Ar_2^*(^3\Sigma_u^+)$, while the more slowly decaying component of the absorption is due almost entirely to Ar_2^* ($^3\Sigma_u^+$) alone. Guided by the magnitudes of the cross sections reported for the excited states of Ar[40] and for Ar trimer ions,[42–44] numerical experimentation has shown that both the magnitude and two-phase time dependence of the observed broadband photoabsorption in Ar (Fig. 14) can be explained satisfactorily in terms of the computed temporal evolution of the species shown in Fig. 15 and the cross sections presented in Table I. Figure 16 shows the fractional contributions to Ar absorption for the conditions of Figs. 14 and 15.

B. Argon-xenon mixtures

Both the magnitude and temporal variation of the measured absorption, particularly the latter, are changed significantly by the addition of a small amount (< 1%) of Xe to Ar. Figure 14 shows the measured absorption in Ar containing 16 Torr of Xe for conditions similar to those of pure Ar. The maximum value of the absorption is lowered slightly to about 7% cm^{-1} with Xe present, and occurs about ~40–50 nsec after the excitation pulse. Moreover, the change in the decay of the absorption is strikingly different from that of Ar alone. Figure 14 shows that the absorption is essentially constant for about the first ~100 nsec after termination of the pulse, subsequently decaying with a time constant of approximately 300 nsec. This behavior can be explained on the basis of the computed excited and ionized species concentrations in the Ar-Xe mixture, which are shown in Fig. 17; the Xe** concentration in this figure represents the grouped 6s', 6p, 5d, and higher lying levels of Xe.

Although the peak values of Ar**, Ar_2^*, and Ar_3^+ are reduced significantly due to rapid excitation and charge transfer to Xe, these species still make an important contribution to absorption during the excitation pulse as shown in Fig. 18. However, upon termination of the pulse, all Ar-related species decay on a ~10 nsec timescale due to strong quenching by Xe. Corresponding Xe-related molecular species that might be expected to exhibit broadband absorption in the visible region, such as Xe_2^* and Xe_3^+, are present only in very small quantities reflecting the small Xe fractional concentration.

Although the Xe*(6s) concentration (not shown in Fig. 17) has essentially the same time dependence as that of Xe**, and an even larger concentration (~10^{16} cm^{-3}), blue/green photons have insufficient energy to photoionize Xe*(6s).

TABLE I. Blue-green photoabsorption cross sections.[a]

Species	Estimates based on this work	Theoretical calculations
Ar**	1.5	1.2 [Ar(3d)][b]
Xe**	2.0	2.3 [Xe(6p)], 2.7 [Xe(5d)][b]
$Ar_2(^3\Sigma_u^+)$	1.0	...
Ar_3^+	2.5	~1.0,[c] ~3.0–4.0[d]

[a] Units are 10^{-17} cm^2.
[b] Reference 40.
[c] Reference 42.
[d] Reference 44.

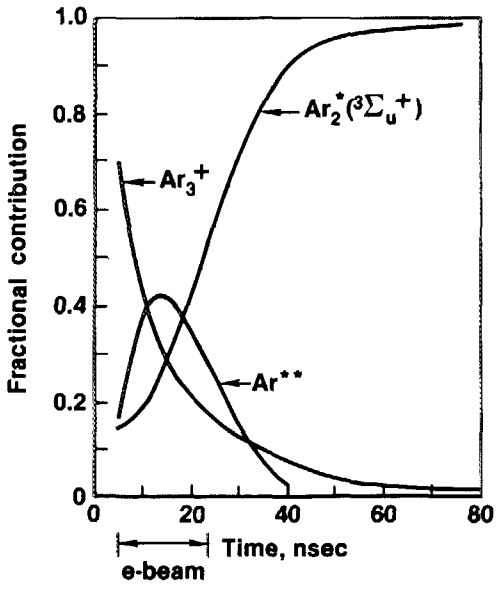

FIG. 16. Computed fractional contributions to the absorption in Ar (Fig. 14), based on the species concentrations of Fig. 15 and the cross sections of Table I.

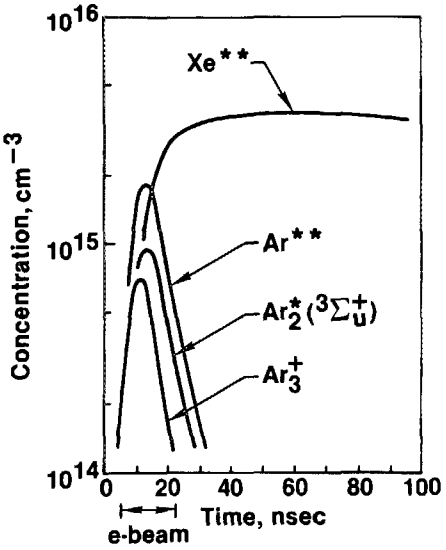

FIG. 17. Computed temporal evolution of certain species concentrations for the Ar-Xe mixture conditions of Fig. 14.

Thus, although discrete phototransitions from Xe* ($^3P_2$, $^3P_1$) to higher levels can be readily identified in the structured spectrum of XeF($C \rightarrow A$) lasers,[17] the very large Xe*(6s) concentration does not contribute *directly* to broadband absorption. However, Duzy and Hyman[40] compute photoionization cross sections for Xe**(6*p*) and Xe**(5*d*) that are approximately 2 and 3×10^{-17} cm^2, respectively, at about 480 nm, varying only slightly throughout the wavelength range of present interest. When these cross section values are considered along with the computed magnitude and time dependence of the Xe** population (Fig. 17), it becomes clear that the observed absorption in the Ar-Xe mixture of Fig. 14 is dominated by photoionization of Xe excited states, most probably those of the 6*p* and 5*d* manifolds. The computed fractional contributions to absorption in the Ar-Xe mixture of Fig. 14, based on the cross sections of Table I, and presented in Fig. 18.

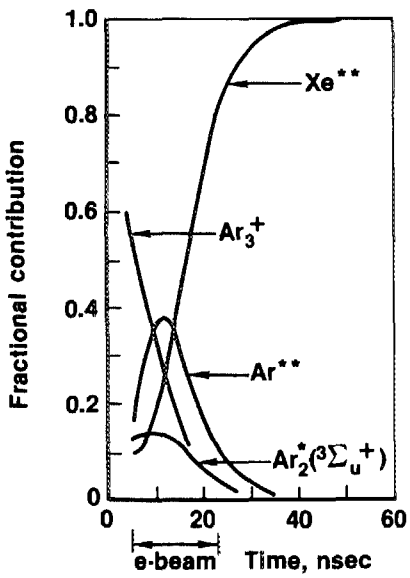

FIG. 18. Computed fractional contributions to the absorption in the Ar-Xe mixture of Fig. 14, based on the species concentrations of Fig. 17 and the cross sections of Table I.

There are several reasons for the unusually large, slowly varying Xe* and Xe** populations for the present Ar-Xe mixture conditions. Modeling shows that the dominant ionized and excited species in the afterglow are atomic (i.e., Xe^+, Xe*, and Xe**), even though the total pressure is very high. Since the Xe fractional concentration is small (< 0.01), the rates of formation of the molecular species Xe_2^* ($^{1,3}\Sigma_u^+$) and Xe_2^+ are much less than those for the corresponding reactions in pure Ar. Further, the heteronuclear species $ArXe^+$ and ArXe* are bound by only 0.14 eV[46] and < 0.1 eV,[26d] respectively, so that the reverse rates for production of Xe^+ and Xe* from these molecular species are large. Consequently, the relative populations of Xe-related molecular species are much smaller than would be expected considering the high total pressure. Because the dominant ion is Xe^+, the electron loss by dissociative recombination is slow, with the result that the electron density in the Ar-Xe mixture remains high after termination of the excitation pulse, unlike the situation in pure Ar. The electrons collisionally mix Xe* and Xe** thereby establishing a quasiequilibrium condition, and, since *both* the production and loss of Xe* and Xe** are dominated by electron collisions, the concentrations of these species are practically time independent in the early afterglow. Therefore, the only significant reaction path away from the coupled Xe*-Xe** system is the relatively slow formation of the excimer Xe_2^* ($^{1,3}\Sigma_u^+$). This process is characterized by a ~ 300 nsec time constant for the present conditions, a value very close to that observed for the absorption decay in the Ar-Xe mixture (Fig. 14).

C. XeF($C \rightarrow A$) laser mixtures

Of course, the excited and ionized species discussed in connection with absorption in Ar and Ar-Xe mixtures will be present in XeF laser mixtures, albeit at significantly lower concentrations. Additionally, there will be other transient species related to F_2 and/or NF_3 such as various rare-gas halides. However, modeling shows that the only additional species having concentration levels that could lead to significant absorption (given appreciable blue/green photoabsorption cross sections) are the triatomic rare-gas halides, Ar_2F and Xe_2F. Calculations by Wadt[47] show that there are several allowed transitions between the lowest energy $RG_2X(2^2B_2)$ state and higher energy states, with peak absorption wavelengths throughout the UV/visible region. However, only the UV transitions analogous to the corresponding RG_2^+ absorption have large oscillator strengths, and are therefore expected to have significant absorption cross sections. Visible transitions in RG_2X, although broadband, have computed oscillator strengths more than one hundred times less than those of the UV transitions, implying peak absorption cross sections having values well below 10^{-18} cm^2. For this reason broadband visible absorption due to the presence of Xe_2F and/or Ar_2F is likely to be unimportant. Thus, we conclude that the same species causing the absorption in Ar and Ar-Xe mixtures (Table I) dominate the absorption in XeF($C \rightarrow A$) laser mixtures.

1. Computed net gain

Presented in Fig. 19 is the net gain computed for conditions similar to those of Fig. 7. The various contributions to the absorption are presented in Fig. 20. Examination of Fig. 19 shows that the net gain for laser conditions can be computed in good qualitative and quantitative agreement with experimental observations using the absorption cross sections inferred by analysis of the absorption in Ar and Ar-Xe mixtures (Table I). Further, it is clear that while all the species identified as absorbers in Ar and Ar-Xe mixtures contribute significantly to absorption in the laser mixture (Fig. 20), photoionization of Xe** is the most important absorption process.

Additional support for this conclusion is provided by absorption measurements using the 590-nm dye laser probe, which indicate a peak absorption of 2.5% cm^{-1}. Since there is no contribution to net gain/absorption from XeF(C) at this wavelength, the measured 2.5% cm^{-1} is actually the *total* absorption coefficient, a value significantly lower than the 4.0%–5.0% cm^{-1} peak value found to be typical of the blue/green region (Fig. 19). However, the 590-nm photon energy is insufficient to ionize either the Xe(6p) levels or the first four Xe(5d) levels. Because relaxation of the higher excited states of Xe by Ar is very fast,[26] it is probable that the 6p and 5d levels dominate the calculated Xe** population. Simply subtracting the Xe** contribution (Fig. 20) reduces the peak absorption coefficient from ~4.0% cm^{-1} (Fig. 19) to about 2.5% cm^{-1}, a value in good agreement with the 590 nm absorption measurement.

D. Laser mixtures with krypton

Figure 10 shows that addition of Kr to the optimum laser mixture reduces the peak absorption from about 2% cm^{-1} to ~0.25% cm^{-1}. Addition of the same amount of Kr to Ar and to the Ar-Xe mixture was found to reduce the absorption of the former by over 50% and to have little effect on the latter. This suggests that the presence of Kr in the laser mixture reduces the initial absorption caused by Ar-related species. Excitation transfer from Ar** to Kr results

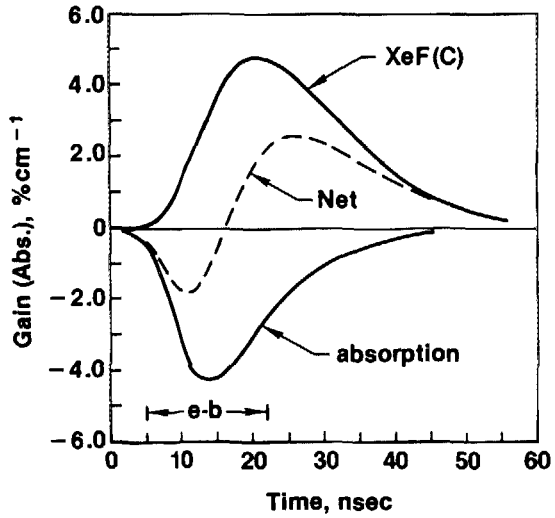

FIG. 19. Gain and absorption at 488 nm for the conditions of Fig. 7, based on computed species concentrations and the cross sections of Table I.

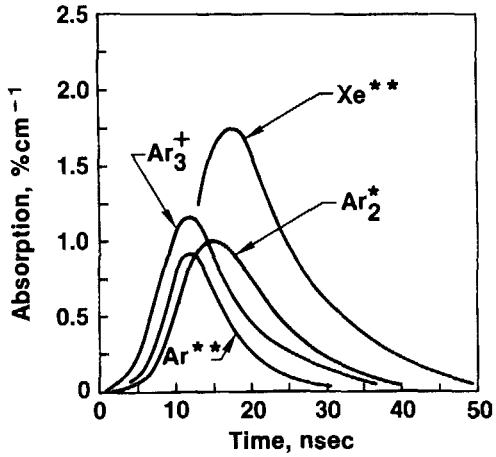

FIG. 20. Computed contributions to the absorption at 488 nm corresponding to the conditions of Fig. 19.

in the production of higher excited states of Kr that have photoionization cross sections somewhat larger than those of the corresponding Ar states.[40] However, excitation transfer from $Ar_2^*(^3\Sigma_u^+)$ can only result in Kr(5s,s') states, while Ar_2^+ and Ar_3^+ charge exchange results in the formation of Kr^+ (or $ArKr^+$) ions. Calculations show that 0.2 atm Kr added to the XeF(C) laser mixture reduces the $Ar_2^*(^3\Sigma_u^+)$ population by approximately a factor of two and the Ar_3^+ population by over an order of magnitude. Examination of Fig. 20 indicates that the corresponding reduction in the contributions of Ar_2^* and Ar_3^+ to absorption could easily account for the experimental observations. However, a comparison of the temporal evolution of the fluorescence for laser mixtures with and without Kr shows that the $C \rightarrow A$ fluorescence rises somewhat faster in the Kr-containing mixture. Krypton is known to be faster than Ar at both relaxing the XeF(B,C) vibrational manifold and at mixing the two states,[16] although it is somewhat surprising if these effects are responsible for the faster XeF(C) fluorescence rise, given the fact that the Ar-Kr ratio was very large in these experiments. In any case, it appears that the dramatic reduction in initial absorption of XeF(C) laser mixtures containing Kr is due primarily to a reduction in the concentrations of Ar-related molecular absorbers, and possibly to an increase in the production rate of XeF(C) as well. Unfortunately, both gain and fluorescence data also show that quenching of XeF(C) is faster with Kr present. Nonetheless the near absence of early absorption with Kr added and peak net gain values comparable to the highest measured may have significant implications for improving laser extraction efficiency.

VI. LASER EFFICIENCY

A. e-beam energy deposition

Determination of the electrical-optical energy conversion efficiency corresponding to the measured laser pulse energy requires knowledge of the e-beam energy deposition in the gas. Several three-dimensional computer models[48–50] of e-beam energy deposition, and measurements[48] of gas pressure rise, all show that the energy deposited under conditions similar to those of this investigation typically is from

two to four times greater than that computed on the basis of simple stopping power calculations. The difference is due largely to backscatter from the cell walls and to multiple scattering in the foil separating the low and high pressure regions of the cell. To account for such effects, in this work we have used a factor of three correction to a stopping power calculation based on the Berger and Seltzer data[51] in order to obtain a reasonable estimate of the *e*-beam energy deposited in the active volume. Measured current density levels on the optical axis were found to vary from 200 to 400 A cm^{-2}, depending on *e*-beam control parameters and unpredictable shot to shot variations. This range of current density, combined with Ar pressures in the 6-10 atm range, corresponds to energy deposition levels ranging from approximately 100 to 300 J/liter depending upon the specific combination of conditions. Therefore, our highest measured laser pulse energies of 1.0-2.0 J/liter correspond to an intrinsic laser efficiency of about 0.5%–1.0%. Although such estimates of *e*-beam energy deposition have to be considered somewhat uncertain, calculations of peak XeF(C) population, net gain, and the temporal relationship among laser medium properties, all of which depend on the modeling of *e*-beam energy deposition, are found to be in good agreement with experimental observations. Thus, we conclude that the *e*-beam energy deposition so estimated is probably accurate to within about $\pm$ 35%, a level of uncertainty that must also be assigned to the inferred value of intrinsic laser efficiency.

B. Optical extraction efficiency

Presented in Fig. 21 is the computed temporal evolution of the intracavity optical flux for typical conditions. The relationship between fluorescence, net gain and laser pulse intensity in this figure is found to be in very good agreement with experiment. This figure shows that although the intracavity flux eventually reaches a level about three times the $\sim$6 MW cm^{-2} saturation flux, resulting in a significant depletion of the tail of the XeF(C) population profile, collisional deactivation of the C state still dominates the time integrated XeF(C) population decay. Thus, although the XeF(C) formation efficiency is 5%–7%, the overall optical extraction efficiency is only about 10%, a factor presently limiting the intrinsic laser efficiency to a value somewhat less than 1%.

The key factor limiting extraction efficiency is the strong initial abosrption occurring during the excitation pulse. In spite of a significant increase in net gain and gain-absorption ratio over prior levels, even for conditions for which the highest output energy has been obtained, the gain does not become positive until after the excitation pulse is terminated. Further, the maximum value of gain is only slightly higher than one half that based on the XeF(C) population alone (Fig. 19). Calculations show that in the absence of such absorption, the intracavity flux would rise rapidly to a level approximately ten times the saturation flux at about the time the maximum zero-field XeF(C) population is achieved, a circumstance that would result in an extraction efficiency of approximately 40% for the conditions of this experiment. This suggests that even though addition of Kr to the optimum Ar-Xe-NF_3-F_2 mixture did not increase the

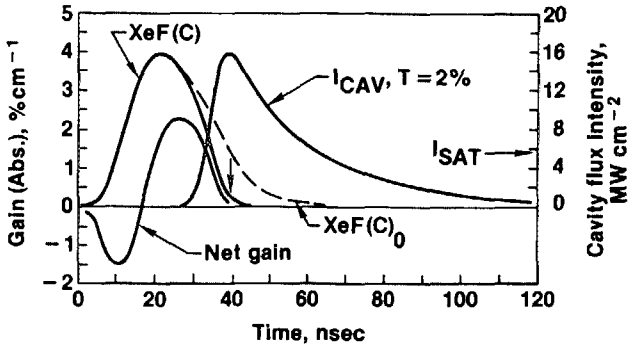

FIG. 21. Temporal evolution of net gain, intracavity optical flux, and XeF(C) population with and without the cavity flux, computed for conditions similar to those of Figs. 7 and 19. The transmission of the output mirror was 2%.

single pulse laser energy density, the near absence of initial absorption (Fig. 10) in certain Kr-containing mixtures may permit significant improvement in extraction efficiency if a multiple pulse excitation scheme is utilized to prolong the gain duration. For example, with a dual-pulse technique, the first pulse would be used to produce a high intracavity flux level prior to initiation of a second, higher energy pulse. Because there is very little initial absorption in Kr-containing mixtures, initiation of the second pulse near the time of the peak flux produced by the first should produce no significant detrimental effect. However, the high cavity flux present at the onset of the second pulse would ensure more efficient energy extraction. Preliminary modeling of conditions representative of this variation on the laser pulse-injection scheme indicate that extraction efficiency levels significantly larger than those obtained to date may be possible.

1. Bleaching of absorbing species

It is interesting to note that because the relevant photoabsorption cross sections (Table I) are significantly larger than the XeF($C \rightarrow A$) stimulated emission cross section, the saturation fluxes for the transient absorbers are about the same as that of XeF(C), in striking contrast to the situation typical of the rare-gas-halide $B \rightarrow X$ lasers. Thus, optical bleaching of the absorbing species is significant for the intracavity flux levels achieved in these experiments. For the conditions of Fig. 21 calculations indicate that the peak cavity flux (and both the laser output energy and efficiency) reach levels approximately 50% higher than would be the case without bleaching of the absorbers.

VII. SUMMARY

Electron-beam excitation of a unique two-halogen gas mixture has been shown to be an effective way to obtain efficient, broadband XeF($C \rightarrow A$) excimer laser oscillation in the blue/green spectral region. Such a laser can now operate at intrinsic energy conversion efficiency approaching one percent with output pulse energy in excess of 1.0 J/liter. These greatly improved laser characteristics have been achieved by careful optimization of the components of the rare-gas-halide mixture, increased electron beam energy deposition, and improved optical resonator design.

Temporal and spectral gain/absorption, laser energy,

and fluorescence measurements under a variety of experimental conditions have provided good insight into the underlying kinetic and spectroscopic processes which control the performance of the XeF($C \rightarrow A$) laser. Excellent agreement between experiment and theory has been demonstrated. The contributions to the major energy pathways resulting in the formation and loss of XeF(C), and to transient photoabsorption in the visible region of the spectrum have been studied in order to characterize the optical extraction and intrinsic laser efficiency.

Broadband molecular and atomic absorption is the most important factor limiting the efficiency of electrically excited XeF($C \rightarrow A$) lasers. For the laser mixtures investigated in this work, the primary absorption processes have been identified as photoionization of the $4p$, $3d$, and higher lying states of Ar, and of the Xe $6p$ and $5d$ states, and photodissociation of $Ar_2(^3\Sigma_u^+)$ and Ar_3^+. These saturable absorbers have blue/green photoabsorption cross sections comparable in magnitude to the XeF($C \rightarrow A$) stimulated emission cross section, and are bleached for intracavity flux levels $\gtrsim 3.0$ MW cm^{-2}, an effect resulting in a prolongation of the gain duration thereby enhancing optical extraction efficiency. Quenching of some of the absorbing species by the addition of F_2 to the Ar-Xe-NF_3 mixture increases the laser efficiency and the output power considerably. Further improvements, such as controlled optical bleaching of the absorbers, additional kinetic refinements, or double pumping, may lead to even higher XeF($C \rightarrow A$) laser efficiencies. Indeed, intrinsic efficiency values approaching those of the UV $B \rightarrow X$ rare-gas-halide lasers seem a distinct possibility.

The stimulated emission cross section for the XeF($C \rightarrow A$) transition is an order of magnitude smaller than that of the $B \rightarrow X$ transition, and, since $\gtrsim 95\%$ of the excited state population of XeF(B,C) is in the XeF(C) level, superradiance in a large scale laser device should be relatively small. Calculations and calibrated fluorescence measurements show that the XeF(C) formation efficiency is 5%–7% for the present conditions. Therefore, the XeF($C \rightarrow A$) excimer medium has the potential to become an efficient wideband, high-power laser amplifier in the blue/green region that could be used as a final amplifier in conjunction with another laser oscillator.

ACKNOWLEDGMENTS

It is a pleasure to acknowledge the contributions of Professor D. W. Setser of Kansas State University and those of Dr. R. Tripodi and Dr. H. H. Michels of UTRC. This work was supported in part by the Office of Naval Research, the National Science Foundation and the Robert A. Welch Foundation.

[1](a) D. Kligler, H. H. Nakano, D. L. Huestis, W. K. Bischel, R. M. Hill, and C. K. Rhodes, Appl. Phys. Lett. **33**, 39 (1978); (b) H. Helm, D. L. Huestis, M. J. Dyer, and D. C. Lorents, J. Chem. Phys. **79**, 3220 (1983).
[2]W. E. Ernst and F. K. Tittel, Appl. Phys. Lett. **35**, 36 (1979).
[3]J. D. Campbell, C. H. Fisher, and R. E. Center, Appl. Phys. Lett. **37**, 348 (1980).
[4]4. R. Burnham, Appl. Phys. Lett. **35**, 48 (1979).
[5]C. H. Fisher, R. E. Center, G. J. Mullaney, and J. P. McDaniel, Appl. Phys. Lett. **35**, 26 (1979).
[6]W. K. Bischel, H. H. Nakamo, D. J. Eckstrom, R. M. Hill, D. L. Huestis, and D. C. Lorents, Appl. Phys. Lett. **34**, 565 (1979).
[7]W. K. Bischel, D. J. Eckstrom, H. C. Walker, Jr., and R. A. Tilton, J. Appl. Phys. **52**, 4429 (1981).
[8]D. J. Eckstrom and H. C. Walker, IEEE J. Quantum Electron. **QE-18**, 176 (1982).
[9]C. H. Fisher, R. E. Center, G. J. Mullaney and J. P. McDaniel, Appl. Phys. Lett. **35**, 901 (1979).
[10]J. Liegel, F. K. Tittel, and W. L. Wilson, Jr., Appl. Phys. Lett. **39**, 369 (1981).
[11]J. C. Hsia, J. A. Mangano, J. H. Jacob, and M. Rokni, Appl. Phys. Lett. **34**, 208 (1979).
[12]W. L. Nighan, Y. Nachshon, F. K. Tittel, and W. L. Wilson, Jr., Appl. Phys. Lett. **42**, 1006 (1983).
[13]D. J. Spencer, J. Appl. Phys. **49**, 3729 (1978).
[14]J. E. Velazco, J. H. Kolts, and D. W. Setser, J. Chem. Phys. **69**, 4357 (1978).
[15]J. E. Velazco, J. H. Kolts, and D. W. Setser, J. Chem. Phys. **65**, 3468 (1976).
[16](a) H. C. Brashears and D. W. Setser, J. Chem. Phys. **76**, 4932 (1982); (b) Y. C. Yu, D. W. Setser, and H. Horiguchi, J. Phys. Chem. **87**, 2199 (1983).
[17]R. Sauerbrey, F. K. Tittel, W. L. Wilson, Jr., and W. L. Nighan, IEEE J. Quantum Electron. **QE-18**, 1336 (1982).
[18]We observe higher peak absorption at 514.5 nm than at any other wavelength both in Ar and in laser mixtures (Fig. 11). Zamir and co-workers (Ref. 36) report similar behavior in e-beam excited Ar at high pressure. They suggest that the structure observed at 514.5 nm is due to the bound-bound $4s^3\Sigma_u^+ - 5p^3\pi_g$ transition in Ar. Although the time dependence of the 514.5 nm absorption reported in Ref. 36 seems to be consistent with the anticipated $^3\Sigma_u^+$ decay, it is difficult to assign the absorption to the $^3\Sigma_u^+ - {}^3\pi_g$ transition in view of the potential curves reported by Yates *et al.* (Ref. 45).
[19]M. R. Flannery and T. P. Tang, Appl. Phys. Lett. **32** 327, 356 (1978).
[20]W. Lowell Morgan, B. L. Whitten, and J. N. Bardsley, Phys. Rev. Lett. **45**, 2021 (1980).
[21]R. Sauerbrey, W. Walter, F. K. Tittel, and W. L. Wilson, Jr., J. Chem. Phys. **78**, 735 (1983).
[22]D. K. Bohme, N. G. Adams, M. Moseman, D. B. Dunkin, and E. E. Ferguson, J. Chem. Phys. **52**, 5094 (1970).
[23]C. B. Collins and F. W. Lee, J. Chem. Phys. **71**, 184 (1979).
[24]W. J. Wiegand, Jr., in *Applied Atomic Collision Physics*; *Volume 3*: *Gas Lasers*, edited by H. S. W. Massey, E. W. McDaniel, and B. Bederson (Academic, New York, 1982), Chap. 3 and references cited therein.
[25](a) P. Millet, A. Birot, H. Brunet, H. Dijols, J. Galy, and Y. Salamero, J. Phys. B **15**, 2935 (1982); (b) H. Brunet, A. Birot, H. Dijols, J. Galy, P. Millet, and Y. Salamero, J. Phys. B **15**, 2945 (1982); (c) Y. Salamero, A. Birot, H. Brunet, H. Dijols, J. Galy, P. Millet, and J. P. Montagne, J. Chem. Phys. **74**, 288 (1981).
[26](a) H. Horiguchi, R. S. F. Chang, and D. W. Setser, J. Chem. Phys. **75**, 1207 (1981); (b) R. S. F. Chang and D. W. Setser, J. Chem. Phys. **69**, 3885 (1978); (c) R. S. F. Chang, H. Horiguchi, and D. W. Setser, J. Chem. Phys. **73**, 778 (1980); (d) J. H. Kolts and D. W. Setser, J. Chem. Phys. **68**, 4848 (1978).
[27]P. J. Chantry, in *Applied Atomic Collision Physics*; *Volume 3*: *Gas Lasers*, edited by H. S. W. Massey, E. W. McDaniel, and B. Bederson (Academic, New York, 1982), Chap. 2.
[28](a) W. L. Nighan, IEEE J. Quantum Electron. **QE-14**, 714 (1978); (b) M. Rokni, J. A. Mangano, J. H. Jacob, and J. C. Hsia, IEEE J. Quantum Electron. **QE-14**, 464 (1978); (c) D. L. Heustis, R. M. Hill, H. H. Nakano, and D. C. Lorents, J. Chem. Phys. **69**, 5133 (1978).
[29](a) W. L. Morgan and A. Szoke. Phys. Rev. A 23, 1256 (1981); (b) D. Klimek and J. C. Hsia, J. Appl. Phys. **52**, 5361 (1981).
[30]G. Marowsky, G. P. Glass, F. K. Tittel, K. Hohla, W. L. Wilson, Jr., and H. Weber, IEEE J. Quantum Electron. **QE-18**, 898 (1982).
[31]A. V. Hazi, T. N. Rescigno, and A. E. Orel, Appl. Phys. Lett. **35**, 477 (1979).
[32]L. F. Champagne, in *Applied Atomic Collision Physics*; *Volume 3*: *Gas Lasers*, edited by H. S. W. Massey, E. W. McDaniel, and B. Bederson (Academic, New York, 1982), Chap. 12 and references cited therein.
[33]M. Rokni and J. H. Jacob, in *Applied Atomic Collision Physics*; *Volume 3*: *Gas Lasers*, edited by H. S. W. Massey, E. W. McDaniel, and B. Bederson (Academic, New York, 1982), Chap. 10.
[34]G. M. Schindler, IEEE J. Quantum Electron. **QE-16**, 546 (1980).

[35]D. Eimerl, J. Appl. Phys. **51**, 3008 (1980).
[36]E. Zamir, D. L. Huestis, H. H. Nakano, R. M. Hill, and D. C. Lorents, IEEE J. Quantum Electron. **QE-15**, 281 (1979).
[37]D. L. Turner and D. C. Conway, J. Chem. Phys. **71**, 1899 (1979).
[38]J. A. MacDonald, M. A. Biondi, and R. Johnsen, J. Phys. B **16**, 4273 (1983). The electron recombination coefficient for Ne_3^+ has been measured and found it to be approximately five times larger than that of Ne_2^+, the recombination coefficients for both ions having about the same electron temperature dependence. In the present work, we have assumed that the recombination coefficients for Ar_3^+ and Ar_2^+ are in the same ratio as those of the Ne ions.
[39]J. W. Keto, R. E. Gleason, Jr., and G. K. Walters, Phys. Rev. Lett. **33**, 1365 (1974).
[40]C. Duzy and H. A. Hyman, Phys. Rev. A **22**, 1878 (1980).
[41]H. H. Michels, R. H. Hobbs, and L. A. Wright, J. Chem. Phys. **71**, 5053 (1979).
[42]H. H. Michels, R. H. Hobbs, and L. A. Wright, Appl. Phys. Lett. **35**, 153 (1979).
[43]W. R. Wadt, Appl. Phys. Lett. **38**, 1030 (1981).
[44]The Ar_3^+ photoabsorption cross section estimate reported in Ref. 42 is based on a triangular ionic structure. However, there is evidence that the most stable structure for Ar_3^+ is linear (Refs. 37 and 43). On this basis the cross section for photodissociation of Ar_3^+ is estimated to be approximately $3\text{–}4\times10^{-17}$ cm^2 in the blue/green region [H. H. Michels (private communication)].
[45]J. H. Yates, W. C. Ermler, N. W. Winter, P. A. Christiansen, Y. S. Lee, and K. S. Pitzer, J. Chem. Phys. **79**, 6145 (1983).
[46]C. Y. Ng, P. W. Tiedeman, B. H. Mahan, and Y. T. Lee, J. Chem. Phys. **66**, 5737 (1977).
[47]W. R. Wadt and P. J. Hay, J. Chem. Phys. **68**, 3850 (1978).
[48]D. J. Eckstrom and H. C. Walker, Jr., J. Appl. Phys. **51**, 2458 (1980).
[49]G. A. Hart and S. K. Searles, J. Appl. Phys. **47**, 2033 (1976).
[50]K. S. Jancaitis and H. T. Powell (unpublished).
[51]M. J. Berger and S. M. Seltzer, in *Studies in Penetration of Charged Particles in Matter*, Nuclear Science Series Report No. 10, NAS-NRC Publ. No. 1133 (National Academy of Sciences, Washington, D. C., 1964).